Towards integration of pyro- and hydrometallurgical unit operations for efficient recovery of battery metals from waste lithium-ion batteries

L. Klemettinen[1], J. Biswas[2], A. Klemettinen[3], J. Zhang[4], H. O'Brien[5], J. Partinen[6] and A. Jokilaakso[7]

1. Staff Scientist, Aalto University, Department of Chemical and Metallurgical Engineering, 00076 Aalto, Finland. Email: lassi.klemettinen@aalto.fi
2. Assistant Professor, IIT Bombay, Powai, Mumbai, Maharashtra 400076, India. Email: biswasj@iitb.ac.in
3. University Teacher, Aalto University, Department of Chemical and Metallurgical Engineering, 00076 Aalto, Finland. Email: anna.klemettinen@aalto.fi
4. Associate Professor, Wuhan University of Science and Technology - The State Key Laboratory of Refractories and Metallurgy, Wuhan 430081, Hubei, P.R. China. Email: zhangjuhua@wust.edu.cn
5. Senior Researcher, Geological Survey of Finland, 02150 Espoo, Finland. Email: hugh.obrien@gtk.fi
6. Doctoral Researcher, Aalto University, Department of Chemical and Metallurgical Engineering, 00076 Aalto, Finland. Email: jere.partinen@aalto.fi
7. Associate Professor, Aalto University, Department of Chemical and Metallurgical Engineering, 00076 Aalto, Finland. Email: ari.jokilaakso@aalto.fi

Keywords: smelting, slag cleaning, leaching, recycling, lithium, cobalt, manganese

ABSTRACT

Waste lithium-ion batteries (LIBs) are important secondary sources of many valuable materials, including Critical Raw Materials (CRMs) defined by the European Union (EU): lithium, cobalt, manganese, and graphite. Additionally, LIBs typically contain nickel and copper, which are classified as Strategic Raw Materials for EU since 2023. In recent years, great effort has been made to develop efficient recycling processes for waste LIBs. Pyrometallurgical processes have been essential in industrial production of metals for many decades. These technologies are relatively mature, with high adaptability for different raw materials. Pyrometallurgical treatment in LIB recycling typically involves the use of smelting processes, in which waste batteries are heated above their melting points and metals are separated through a reduction reaction in the liquid phase. Through this recycling route, cobalt, copper, and nickel can be efficiently recovered in the form of a metal alloy, whereas lithium and manganese are lost in the slag phase.

The goal of this work was to increase the recoveries of valuable battery metals through a combination of hydro- and pyrometallurgical unit operations. First, industrial Li-ion battery scrap underwent a selective sulphation roasting stage, where the aim was to transform $LiCoO_2$ and Mn-oxides into Li, Co and Mn sulphates. After roasting, the battery scrap was leached in distilled water with a solid to liquid ratio of 100 g/L at 60 °C and recovered 95% of Li, 61% of Mn and 35% of Co. After leaching, the solid leach residue was mixed with industrial Ni-slag and biochar, followed by reduction at 1350 °C in argon atmosphere. The high-temperature smelting experiments were conducted as a function of time (5-60 minutes) to investigate the reduction behaviour of battery metals. The results show that Co and Ni from the slag and leach residue can be efficiently recovered in the slag cleaning stage.

INTRODUCTION

Lithium-ion batteries (LIBs) have become extremely important for portable electronics, green energy technologies, electric vehicles, and energy storage systems. Consequently, research related to batteries has drastically increased over last decade (Li *et al*, 2018). Researchers from all over the world are focusing on improving the design of new batteries, developing new battery materials, as well as developing new routes for the recovery valuables from end-of-life LIBs. Waste lithium-ion batteries are important secondary sources of many valuable materials, including Critical Raw Materials (CRMs) defined by the European Union (EU): lithium, cobalt, manganese, and graphite. Additionally, LIBs typically contain nickel and copper, which are classified as Strategic Raw Materials for EU since 2023 (Grohol and Veeh, 2023).

Current developments in the LIB recycling have been described in recent review papers (Makuza *et al*, 2021; Baum *et al*, 2022; Brückner, Frank and Elwert, 2020). Typical recycling processes consist of discharging and mechanical separation followed by pyrometallurgical and/or hydrometallurgical treatment (Neumann *et al*, 2022). To make the battery recycling processes economically more attractive, they can be integrated with already existing primary metal production processes. In our previous studies (Ruismäki *et al*, 2020a; Dańczak *et al*, 2021; Rinne *et al*, 2022), we have investigated the possibility of integrating different battery scrap flotation fractions with pyrometallurgical slag cleaning processes. The slag used in this study came from an industrial nickel flash smelting furnace. It was iron-silicate slag with some magnesia (MgO) and nickel oxide, as well as minor concentrations of Co and Cu (Crundwell *et al,* 2011). As spent lithium-ion batteries typically contain a high concentration of Co and some Ni and Cu, it was proved earlier (Ruismäki *et al*, 2020b) that it is beneficial to mix a battery scrap fraction rich in Co with nickel slag in order to increase the recovery of Co during the slag cleaning process. In the laboratory-scale Ni-slag cleaning process, Ni, Co and Cu from both waste batteries as well as industrial Ni-slag were recovered in metal alloy and matte phases (Ruismäki *et al*, 2020a; Ruismäki *et al*, 2020b; Dańczak *et al*, 2021). Graphite from waste LIBs was found to be an effective reductant for metal oxides and the reduction reactions appeared to be very fast. No additional reductant was needed in the investigated smelting process. However, lithium and manganese were lost in the slag, therefore the need for an additional pre-treatment stage before the smelting process was identified in order to maximise the valuable metal recoveries. It is not economically viable to recover Li and Mn from huge volumes of base metal smelting slags, which means that their recovery must occur before the smelting process.

The aim of this research was to combine pyro- and hydrometallurgical unit operations for efficient recovery of battery metals Co, Ni, Cu, Li and Mn from Li-ion battery scrap. First, industrial Li-ion battery scrap underwent a sulphation roasting step, where the aim was to transform Li- and Co-containing oxides into Li and Co sulphates. As the formed sulphates were expected to be water soluble, the next step was leaching in water. Water leaching was also selected as it excludes the use of hazardous chemicals and leaching conditions. After water leaching, the solid leaching residue was mixed with industrial nickel slag and smelted in reducing conditions in order to recover Ni, Cu and the remaining Co. Biochar was used as a reductant in the smelting stage, and the experiments were conducted at 1350 °C for different times (5-60 minutes) to investigate the reduction behaviour of the metals of interest as a function of time. The data provided in this study will be useful for integrating Li-ion battery recycling with already existing industrial-scale unit processes.

EXPERIMENTAL

Sulphation roasting

The main raw material for this study was LCO-rich lithium-ion battery scrap, supplied by AkkuSer Oy (Finland), where the samples were pretreated with a dry technology – two stages of crushing followed by magnetic and mechanical separation (Pudas, Erkkilä and Viljamaa, 2015). A size fraction of <125 µm was separated from the industrial scrap by sieving and employed for the current study. The chemical composition of the battery scrap fraction used in the experiments is presented in Table 1.

For each experiment, a batch of 4 g battery scrap was placed in a silica boat in the cold zone of a horizontal tube furnace (Lenton, UK) with a hot zone temperature of 850 °C, after which the furnace was sealed and Ar gas flow (500 mL/min) was started. An ejector was used for creating an underpressure inside the furnace. After approximately 5 minutes, the sample was pushed to the hot zone in three stages, keeping a 2-minute pause between the stages to avoid crucible cracking, followed by changing the gas mixture to 10% SO_2 - 10% O_2 - Ar gas when the sample reached the hot zone. These conditions were selected based on our previous investigation with LCO-rich black mass (Biswas *et al*, 2023). According to the thermodynamic stability diagram (Biswas *et al*, 2023), it was expected that all lithium and cobalt transform into sulphates, whereas other metals should remain as oxides. After 60 minutes of sulphation roasting, the samples were taken out of the furnace following the same three-stage procedure as previously. In total, four roasting experiments were conducted with the same parameters. The roasted battery scrap was analysed using X-ray diffraction technique (X'Pert Pro MPD, PANanalytical, Netherlands) with a scan rate of 2°/min for 10° to 90° angles using Cu-K_α radiation and HighScore Plus software (version 4.8, PANanalytical).

TABLE 1 - Li-ion battery scrap composition before sulphation roasting.

Element	Al	Co	Cu	Fe	K	Li	Mg	Mn	Na	Ni	P	C	Rest
wt%	1.64	26.45	2.72	0.61	0.05	3.87	0.09	1.67	0.06	2.74	0.45	33	26.65

Water leaching

The sulphation roasted samples were mixed together and a 10 g batch was leached in distilled water for 60 minutes with a solid to liquid ratio of 100 g/L at 60 °C and with magnetic stirring at 300 rpm. After leaching, the residue was filtered and the concentrations of metals were analysed by atomic absorption spectroscopy (AAS, Thermo Scientific iCE 3000, USA) after digesting a part of the residue in concentrated aqua-regia (HCl (37%, Merck) and HNO_3 (65%, Merck Supelco) at 3:1 molar ratio). AAS was used for the leaching solution analysis as well. The solid residue was also analysed using the X-ray diffraction technique described in the previous section.

Smelting

The smelting experiments were conducted under simulated conditions of an industrial Ni-slag smelting process. Industrial Ni-slag (Table 2) was used in the experiments. The main reductant in the experiments was biochar prepared from black pellets by pyrolysing at 600 °C, obtained from

University of Oulu (Finland), containing 76.6 wt% carbon. The biochar was supplied as pellets, but it was ground in a mortar into fine powder before the experiments in order to increase the reactive surface area. Detailed analysis of the biochar has been presented previously (Attah-Kyei *et al*, 2023).

TABLE 2 - Chemical compositions of the Ni-slag and concentrate used in the experiments.

Slag, concentrations in wt%													
Fe_3O_4	**Fe**	**Si**	**Ni**	**Mg**	**Ca**	**Al**	**Cu**	**Co**	**Na**	**K**	**Ti**	**S**	**Mn**
20	35.42	10.61	3.41	3.16	0.91	0.84	0.69	0.43	0.35	0.32	0.21	0.16	0.03
Concentrate, concentrations in wt%													
2	29.32	9.25	8.06	2.79	1.05		1.85	0.31				24.41	

Two series of experiments were conducted. In series A, 90 wt% of Ni-slag was mixed with 10 wt% leaching residue. In series B, 5 wt% of the slag was replaced with industrial sulphidic Ni-concentrate (Table 2). The stoichiometric amount of carbon required for complete reduction of NiO to Ni, CuO to Cu, CoO to Co and magnetite (20 wt% in slag) to FeO was calculated, assuming the reaction gas to be CO, and 1.25 times the stoichiometric amount was used in both series. For both series, enough reagents for 5 experiments were weighed and thoroughly mixed in an agate mortar. After mixing, 1.0 g of the mixture was used in each experiment. The weight ratios in the final mixtures were 85.97 / 9.55 / 4.48 for slag / leaching residue / biochar in series A and 81.30 / 9.56 / 4.78 / 4.36 for slag / residue / concentrate / biochar in series B, respectively. The small difference in the amount of biochar is due to the concentrate used in series B, which was already sulphidic and therefore did not require reductant.

The experiments were conducted in a vertical tube furnace (Lenton, UK). 1.0 grams of starting mixture was placed in a conical silica crucible and attached to Kanthal A-wire hanging from inside the furnace. The sample was first lifted to the cold zone of the furnace, followed by closing the furnace work tube with a rubber plug. Next the furnace was flushed with Argon (300 mL/min) for 15 minutes before lifting the sample to the hot zone at 1350 °C and keeping there for 5, 10, 30 or 60 minutes. After the set time, the sample was rapidly quenched to ice-water mixture without breaking the inert atmosphere. Before characterization, the samples were mounted in epoxy, cut in a half by a diamond cutting wheel, mounted in smaller epoxy moulds, ground, and polished with traditional wet metallographic methods. After polishing, the sample surfaces were coated with carbon for microstructural and compositional characterization.

The sample microstructures and elemental compositions of phases were characterized using a scanning electron microscope (SEM; Mira 3, Tescan, Czech Republic) coupled with an energy dispersive spectrometer (EDS; Thermo Fisher Scientific, USA). The beam current was approximately 10 nA and the acceleration voltage was 15 kV. The elemental analyses were conducted using standards supplied by Astimex, as shown in Table 3.

Trace and minor element concentrations in the slags were below reliable detection with EDS, therefore the slags were analysed using laser ablation-inductively coupled plasma-mass spectrometry (LA-ICP-MS). The laser spot size was set to 40 µm with 50 µm preablation and the laser energy was 40.1% of 5 mJ. The fluence, i.e., energy delivered per unit area, was 1.25 J/cm^2 on the sample surface. The laser was operated at 10 Hz frequency and 40 s of ablation data was collected from each spot. NIST610 glass (Jochum *et al*, 2011) was used as an external standard, ^{29}Si (from EDS) as the internal standard. NIST612, USGS BHVO-2G and BCR-2G glasses (Jochum *et al*, 2005) were analysed as unknowns. The obtained time-resolved analysis signals were treated with Glitter software (Van Achterberg *et al*, 2001), and the detection limits are shown in Table 3.

TABLE 3 - EDS standards as well as LA-ICP-MS detection limits. Ppmw = parts-per-million by weight.

Element	EDS Standard	LA-ICP-MS isotope and detection limit (ppmw)
O	Diopside	
Mg	Magnesium	
Al	Aluminium	
Si	Quartz	
S	Marcasite	
Ca	Fluorite	
Fe	Hematite	
Co	Cobalt	^{59}Co: 0.02
Ni	Nickel	^{60}Ni: 0.21
Cu	Copper	^{65}Cu: 0.04
Mn		^{55}Mn: 0.09
Li		^{7}Li: 0.04

RESULTS AND DISCUSSION

Sulphation roasting and water leaching

The XRD pattern of the LCO-rich black mass in Figure 1 suggests that there are two main phases, $LiCoO_2$ and graphite, which originate from the cathode and anode, respectively. The elemental analysis of the black mass in Table 4 also shows 26.6 wt% of Co and 3.87 wt% Li along with small concentrations of Ni, Mn and Cu, confirming this as LCO-rich black mass. At the first stage of this study, the LIB black mass samples were roasted using 10% SO_2 – 10% O_2 – Ar gas flow at 850 °C for 60 minutes. The XRD pattern of the sulphation roasted powder in Figure 1 confirms the formation of Li and Co sulphates, while a fraction of Co could be observed to remain as oxide. $LiCoO_2$ peaks were not observed in the roasted powder sample, indicating a high degree of sulphation (and partial transformation into CoO as observed in the XRD graph). The carbon peak also disappeared after sulphation roasting, suggesting full combustion of carbon. At this temperature, it is also expected that the binders, plastics and organic electrolytes are removed during the roasting process.

After roasting, the samples were leached with distilled water, where the water-soluble metal sulphates were expected to dissolve, leaving metal oxides in the residue phase. The elemental composition of the leach residue, obtained from the water leaching process, is presented in Table 4. The residue consisted of approximately 43 wt% Co, 6 wt% Ni, 6 wt% Cu and low concentrations of Fe, Li and Mn. The XRD pattern of the water leached residue in Figure 1 shows several strong peaks of CoO along with few peaks of $Li_2Co(SO_4)_2$ and $CoSO_4$. This indicates that majority of Li and a fraction of Co were extracted during the water leaching stage. A longer period of water leaching could have been beneficial for the extraction of remaining sulphates. The composition of the residue shows that it contains valuable metals in high concentrations, and it will be a very good raw material for Ni-slag cleaning furnace, where an alloy containing mostly Ni and Co (as well as Fe) is formed.

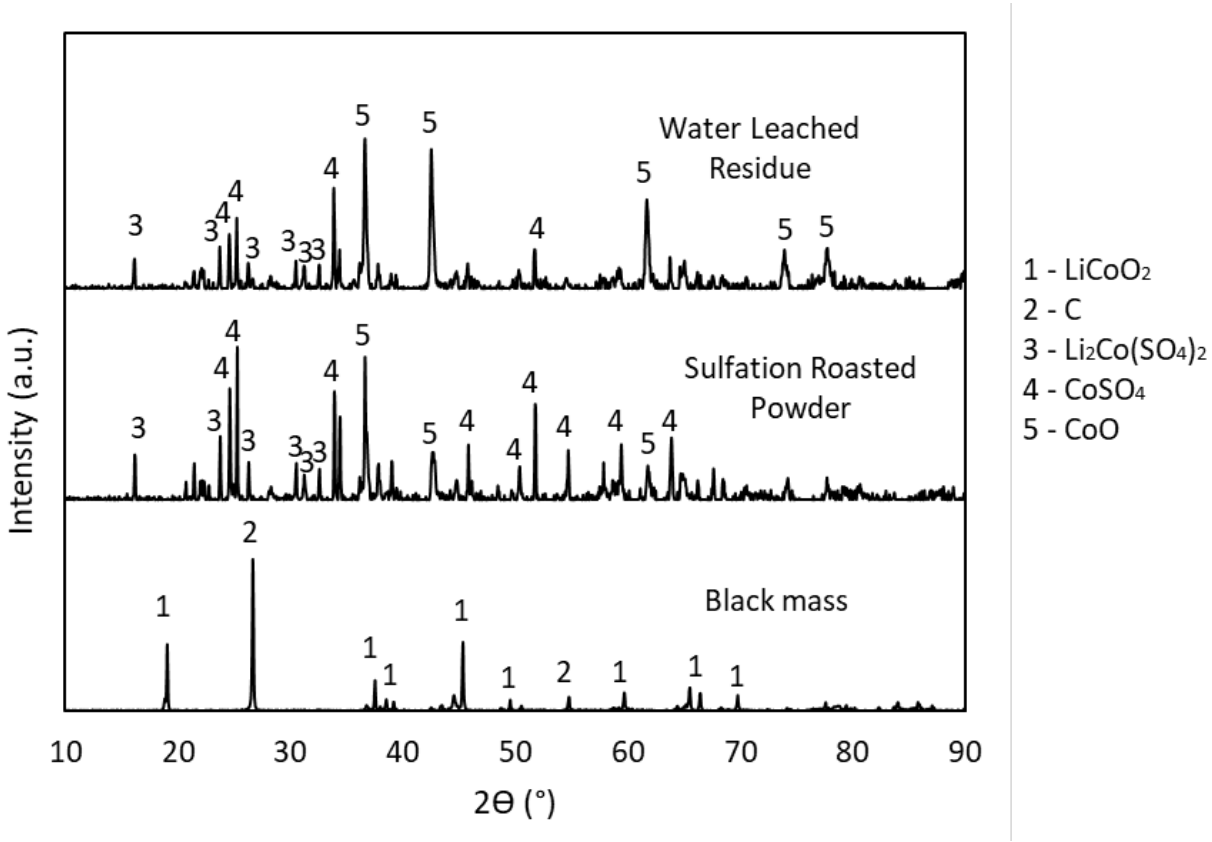

FIG 1 - XRD patterns of black mass, sulphation roasted powder and leach residue after water leaching.

TABLE 4 - Elemental composition of black mass and leach residue. The chemical analysis is based on sample digestion in concentrated aqua-regia, followed by atomic absorption spectroscopy.

Element	Co	Ni	Mn	Cu	Fe	Li	Others
black mass, wt.%	26.45	2.74	1.67	2.72	0.61	3.87	61.94
leach residue, wt. %	43.00	6.10	1.40	6.00	0.20	0.20	43.1

The extraction yields of different metals after leaching, presented in Table 5, were calculated based on metal concentrations in water-leached solution and residue digested solution obtained from AAS analyses. Equation (1) was used in the calculations:

$$\%\, Extraction = \frac{m_1}{m_{1+}m_2} \cdot 100\% \quad (1)$$

where m_1 is the total mass of the specific metal dissolved in water during leaching and m_2 is the total mass of the specific metal remaining in the residue.

Based on the results, approximately 95% of Li, 61% of Mn and 36% of Co were extracted from the black mass in the water leaching stage. According to the thermodynamic stability diagram (Biswas *et al*, 2023), Mn should remain as oxide in the selected roasting conditions, but based on the obtained results, more than half of the Mn-containing oxides were actually transformed to sulphates, as indicated by the 61% extraction efficiency. The surprisingly high Mn extraction during water leaching is beneficial because Mn deports to the slag and cannot be recovered in Ni-slag cleaning stage.

In this research, the focus was mostly on the recovery of metals from the leach residue through Ni-slag cleaning process. The precipitation and purification of metal compounds from the leaching solution was not investigated.

TABLE 5 - Recoveries of metallic elements after sulphation roasting and water leaching.

Element	Co	Ni	Mn	Cu	Fe	Li
Solution after leaching, mg	1130	28	103	12	<1	198
Leach Residue, mg	2051.1	291.0	66.8	286.2	9.5	9.5
% Extraction	35.5	8.8	60.7	4.0	<9.5	95.4

Smelting

The leaching residue was mixed with industrial nickel slag and subjected to a laboratory-scale Ni-slag cleaning process, as described in the Experimental section. SEM images of sample microstructures after smelting in reducing conditions are presented in Figure 2. A typical microstructure consists of the silica crucible (dark grey), glassy slag (medium grey) and matte/metal alloy phase (white). The matte phase had a round shape and was typically found near the bottom of the crucible. In samples without Ni-concentrate (series A, Figure 2 a-b), the matte phase seemed much smaller than in the samples with Ni-concentrate (series B, Figure 2 c-d). Additionally, in the samples without Ni-concentrate, a metal alloy phase was found mostly on the top of the slag layer, which is in line with previous studies on integrating battery scrap recycling with Ni-slag cleaning process (Ruismäki *et al*, 2020a; Dańczak *et al*, 2021).

Besides the largest matte phase area close to the bottom of the crucible, some smaller round matte droplets were also found in other places of the samples. In both series, the smaller matte droplets increasingly coalesced with the largest droplet as the reduction time was increased.

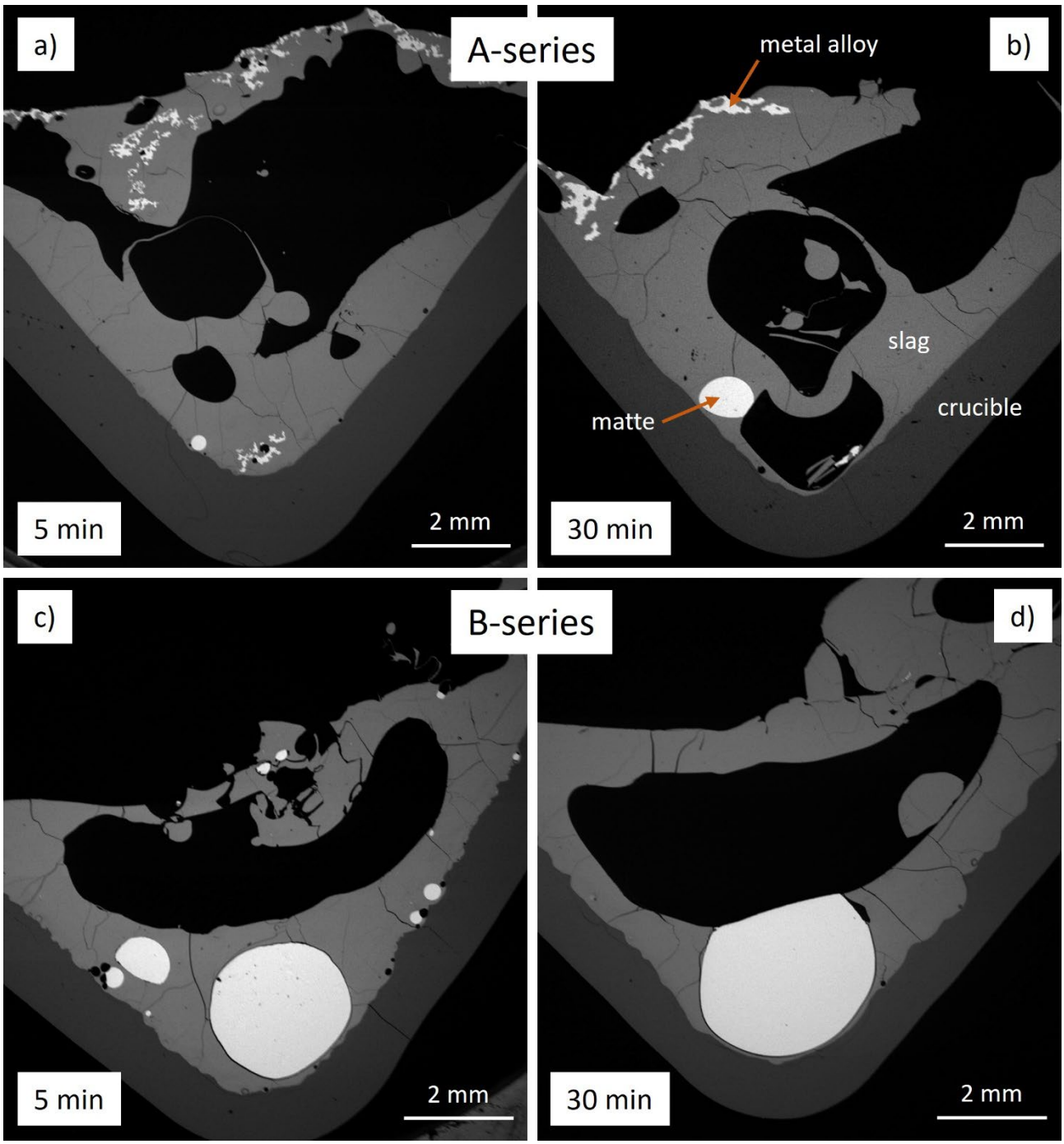

FIG 2 - Microstructures of samples after different reduction times. Figures a) and b) are from series A, while c) and d) are from series B.

A higher magnification SEM-BSE image of a typical microstructure of the matte phase is shown in Figure 3 a, and a typical microstructure of the Fe-rich metal alloy present on top of the slag in the samples without Ni-concentrate is shown in Figure 3 b. Within the whole matte phase, three different phase areas were distinguished, as marked in Figure 3 a: area 1) was metallic Ni-Fe-Co alloy, area 2) was Cu-Ni-Fe sulphide and area 3) was Fe-Ni-Co sulphide. The metal alloy shown in Figure 3 b consisted mainly of Fe-Co-Ni alloy, with minor sulphide areas segregated at the grain boundaries.

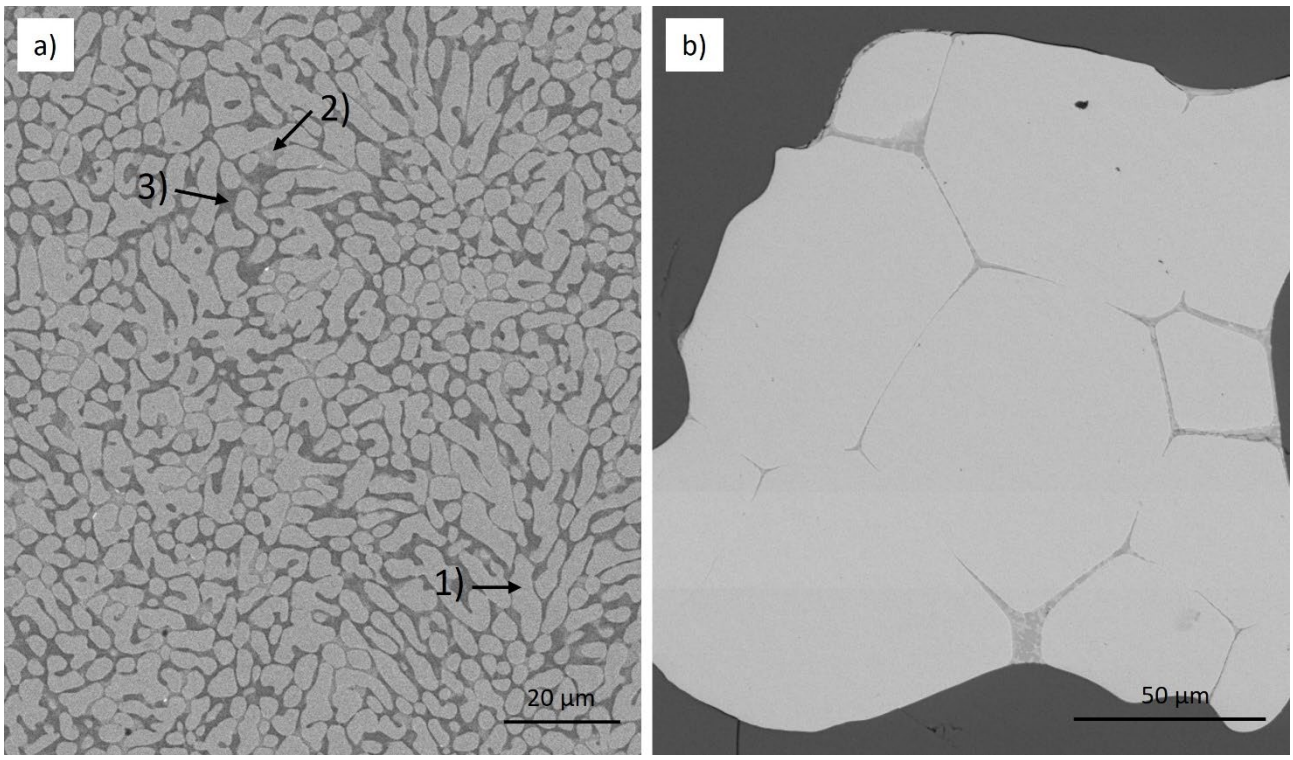

FIG 3 - Microstructure of a) matte, showing three separate phase areas; b) Fe-rich metal phase formed on top of the slag in series A. Both images are from the sample reduced for 10 minutes.

Chemical composition of the slag phase

The concentrations of Fe and SiO_2 in the slags are presented in Figure 4, left side. In both experimental series, Fe concentration decreased as the reduction time increased, and at the same time the concentration of SiO_2 increased. An increase in SiO_2 concentration in the slag was caused by iron reduction as well as dissolution of the silica crucible during smelting. The presence of Ni-concentrate in the samples resulted in faster rates of SiO_2 concentration increase and Fe decrease compared to the series without concentrate. The concentrations of MgO, Al_2O_3 and CaO in the slags are shown in Figure 4, right side. There are no significant differences between the two series, and the concentrations remain relatively stable after 10 minutes of reduction.

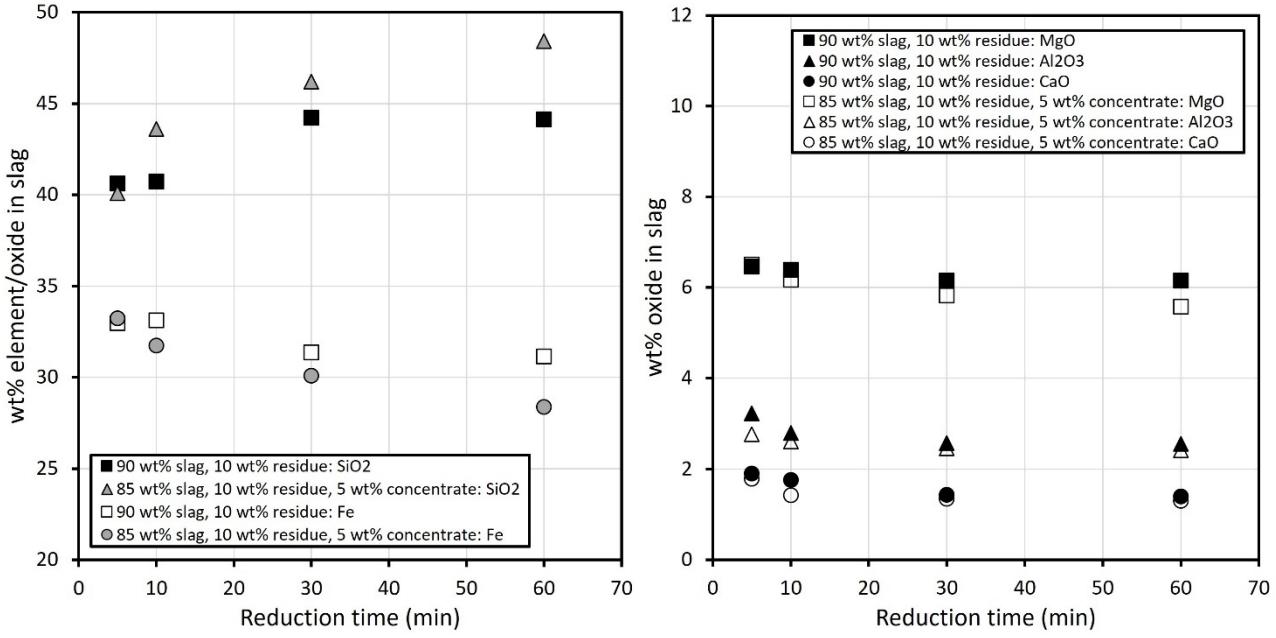

FIG 4 - Concentrations of SiO_2 and Fe (left side) as well as MgO, Al_2O_3 and CaO (right side) in slags after 5-60 min reduction time.

The concentrations of Co, Ni, Cu, Mn and Li in the slag phase are shown in Figure 5. The concentrations of Mn and Li remained relatively constant after 10 minutes. This indicates that the slag volume increase that would have been caused by crucible dissolution, resulting in diluted concentrations of stable oxides such as Li_2O and MnO, was quite effectively compensated by iron reduction from the slag.

The concentrations of Co and Ni decreased significantly as the reduction time increased, especially in series B with Ni-concentrate. The concentration decreases in series A stopped after 30 minutes of reduction, whereas in series B the decrease continued until 60 minutes. At 60 minutes, the concentrations of Ni and Co were lower in series B compared to series A. The concentration of Cu in the slag remained surprisingly constant during the entire reduction time range in series A (without Ni-concentrate). In series B (with Ni-concentrate), a decrease in Cu-concentration was observed as the reduction time increased. Mn and Li originated mostly from the leaching residue, and as the residue amount did not change between the experimental series, neither did their concentrations in the slag significantly.

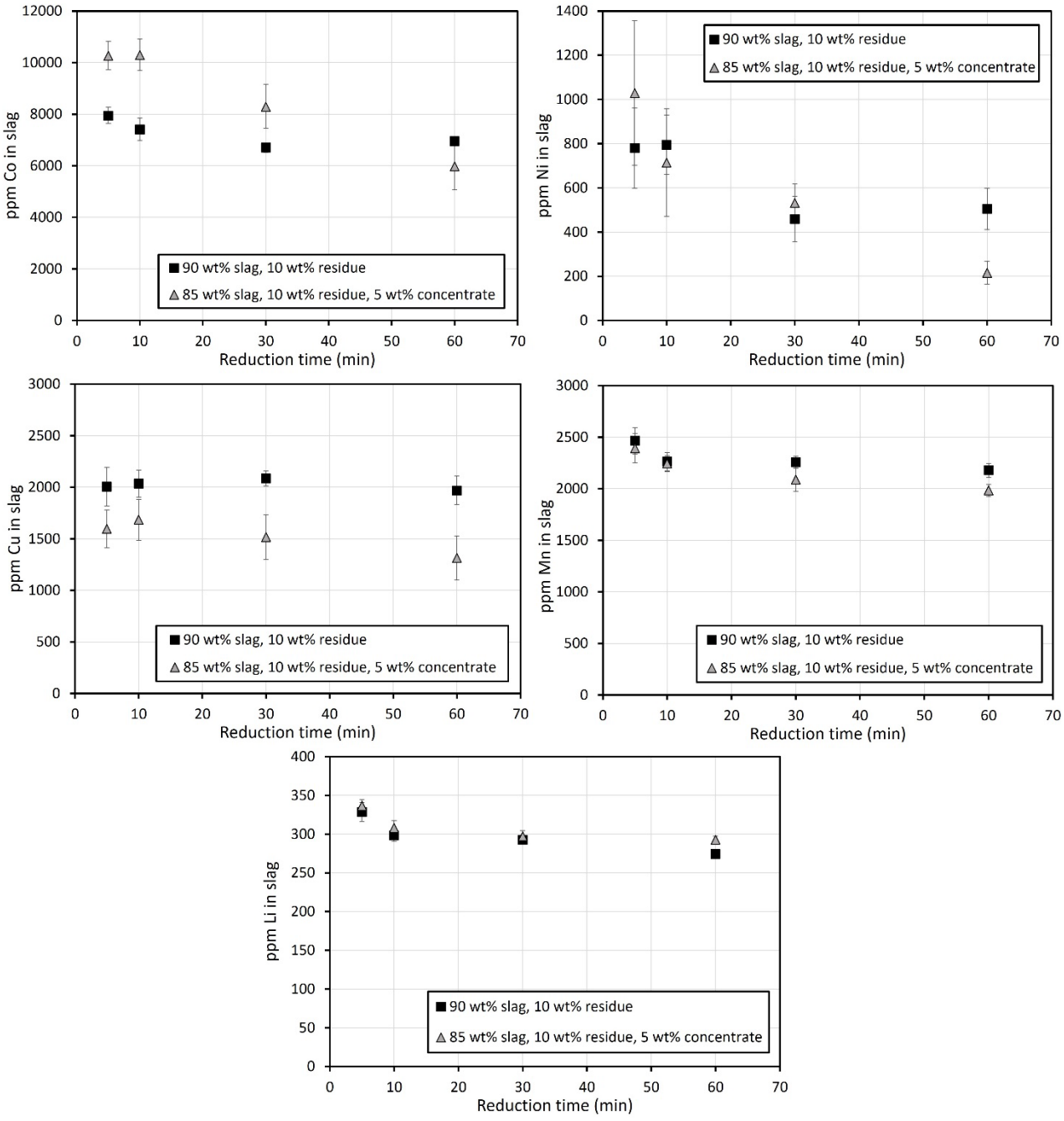

FIG 5 - Concentrations of Co, Ni, Cu, Sn, Pb and Li in slag phase as a function of reduction time at 1350 °C.

Chemical composition of the matte and metal phases

As presented in Figure 3 a, the matte consisted of three different phase areas. The average composition of the matte was calculated according to the method presented by Rinne *et al* (2022). First, the composition of each phase area was analysed using SEM-EDS. Then, several SEM-images were taken from the matte phase of each sample, followed by phase area quantification using ImageJ software and calculation of average composition.

The average concentrations of Fe, Ni, Co, Cu and S in matte after ImageJ calculations are shown in Figure 6. In the series without concentrate, after 10 min reduction, the Ni concentration began to decrease and Fe as well as Co concentrations increased as the reduction time increased. It should be highlighted that even though Ni concentration seems to decrease, it does not mean that the amount of reduced Ni decreased but rather the ratio between Ni and Fe changed as the reduction of iron oxides progressed and the total mass of matte phase increased. The concentrations of Cu and S remained constant after 30 minutes of reduction. The elements in the series with concentrate (Figure 6, right side) behaved differently: at all reduction times, the concentration of cobalt was higher than that of nickel, and the iron concentration did not show an increasing trend as a function of reduction time.

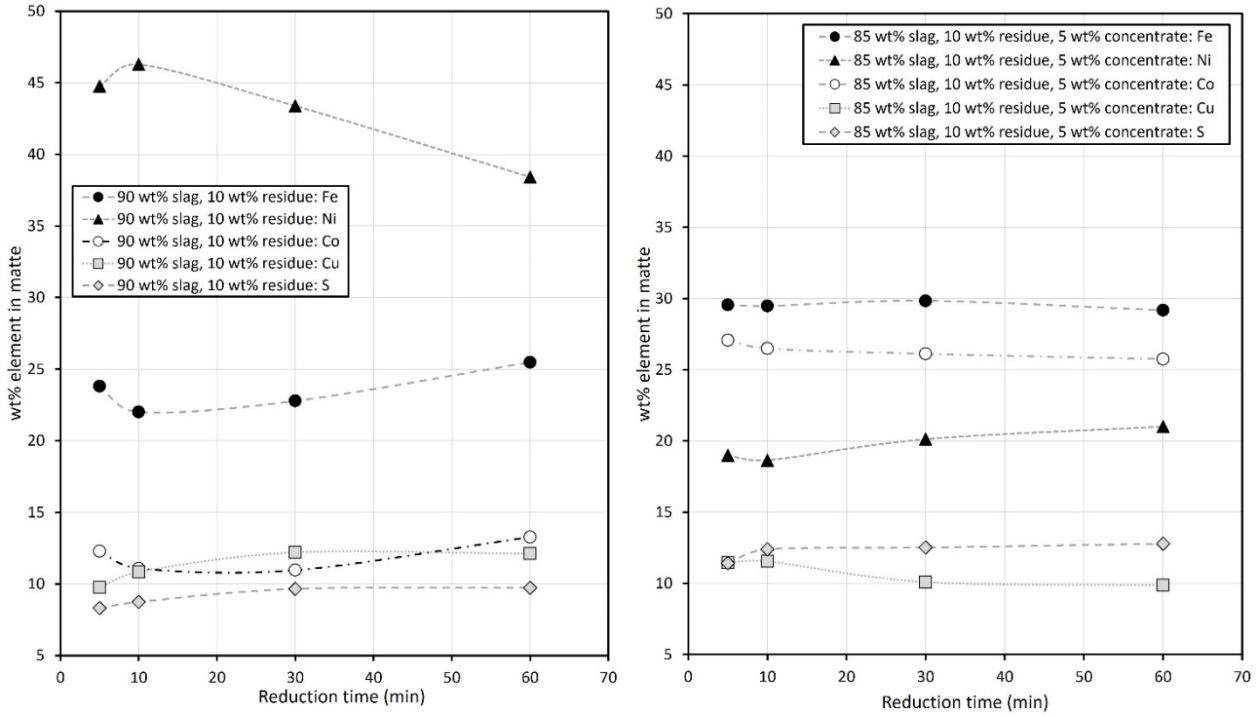

FIG 6 - Concentrations of Fe, Ni, Co, Cu and S in matte as a function of reduction time. Series A on the left side, series B on the right.

The concentrations of iron, nickel, cobalt and copper in the metal phase formed on top of the sample (see Figures 2 a-b and 3 b) in series A, without Ni-concentrate, are presented in Figure 7. This phase is rich in iron and cobalt, which explains the lower iron and cobalt concentrations in the matte phase of this series compared to the series with concentrate, where no metal phase was formed on the sample surface. The elemental concentrations in the metal phase were calculated only based on the concentrations in the metallic grains, excluding the small sulphide areas visible in Figure 3 b. It should be noted that the formation of such a metal alloy on top of the slag is not desirable from industrial perspective, because it cannot be tapped out of the slag cleaning furnace due to not settling below the slag layer.

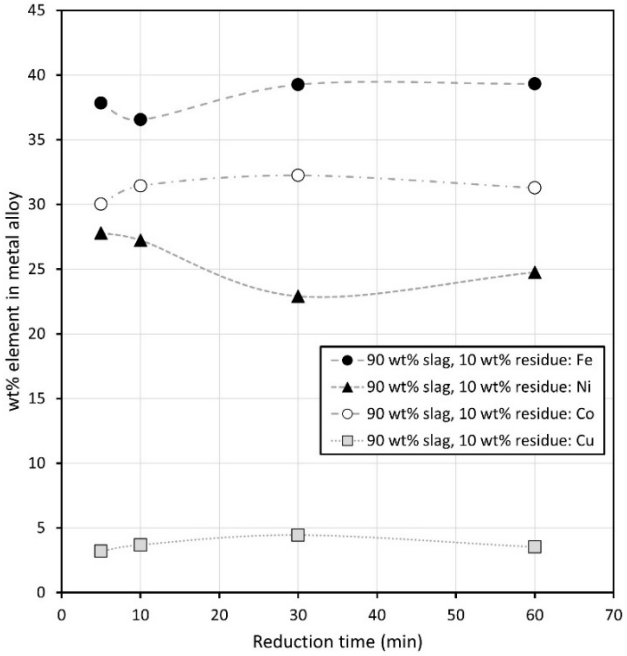

FIG 7 - Concentrations of Fe, Ni, Co and Cu in metal phase of series A.

Distribution coefficients of Co, Ni and Cu between matte and slag

Matte-slag distribution coefficients of Co, Ni and Cu are presented in Figure 8 and were calculated based on equation (2),

$$L^{m/s}Me = [Me\ wt\%]/(Me\ wt\%) \quad (2)$$

where *Me* represents the metal of interest, $L^{m/s}$ is the distribution coefficient of *Me* between matte and slag, [*Me wt%*] is the concentration of *Me* in matte and (*Me wt%*) is the concentration of *Me* in slag.

The distribution coefficient values of Co and Ni increased significantly as the reduction time increased. The recovery of Co in the matte was significantly increased with concentrate addition (series B) compared to series A, as the distribution coefficient value after 60 minutes was approximately 43 compared to 19, respectively. For Ni, the values were systematically higher in the series without concentrate, except for the longest reduction time. In general, the recovery of Ni in matte was approximately 20 times higher compared to Co. The distribution coefficient values for Cu were between 50 and 75, and they did not increase significantly as a function of reduction time. The differences between the two series were relatively small.

The results for Co fit very well with the values obtained previously by Dańczak *et al* (2021) using graphite from battery scrap as a reductant in Ni-slag cleaning. They also reported approximately doubled $L^{m/s}$ Co values when adding Ni-concentrate, compared to without concentrate. Their $L^{m/s}$ Ni values after 60 minutes were approximately 600, which are slightly on the lower side compared to this work. For Cu, Dańczak *et al* reported higher values than obtained in this study, however the trends as a function of time were the same.

Attah-Kyei *et al* (2023) compared the reduction efficiencies of four different biochars with metallurgical coke in Ni-slag cleaning at 1400 °C. The biochar employed in our work was the one which they concluded was the most effective reductant. The distribution coefficient values reported by Attah-Kyei *et al* for Ni after 60 minutes were similar as obtained in this study, for Cu they were somewhat lower and for Co they were 2-3 times higher. A major difference in their work compared to the current study was that only a metal alloy phase was formed and settled at the bottom of the crucible instead of matte phase. Because of this, a direct comparison of distribution coefficient values is not possible.

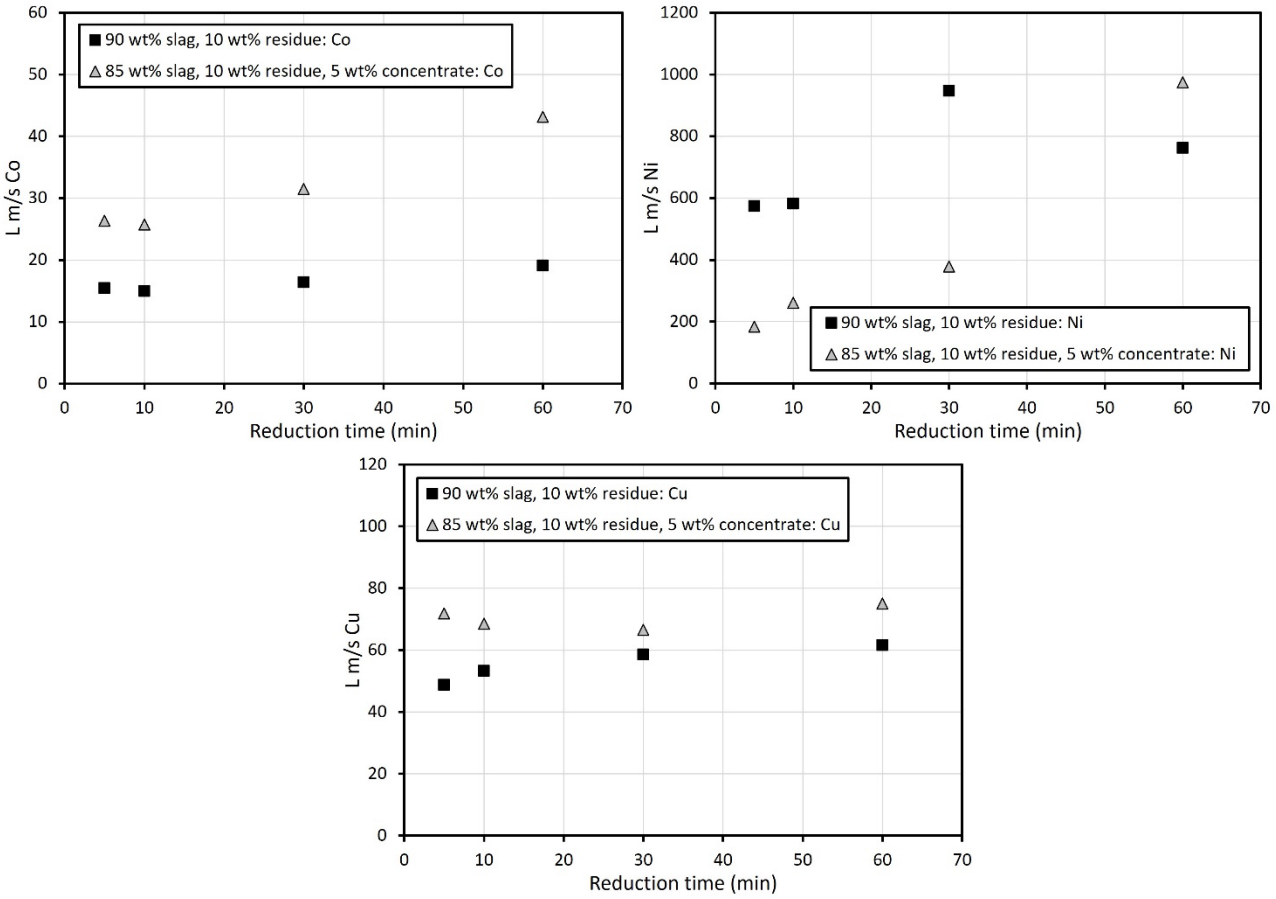

FIG 8 - Matte-slag distribution coefficients of Co, Ni and Cu as a function of reduction time.

CONCLUSIONS

Waste lithium-ion batteries are complex mixtures of chemical elements and their compounds. In order to recover as much valuable metals as possible, smart combinations of mechanical and thermal pretreatment steps as well as pyro- and hydrometallurgical processing are needed. This study is based on the concept that battery recycling could be integrated with already existing technologies for primary metals production.

In this study, the mechanically pretreated battery scrap was subjected to sulphation roasting, where lithium and cobalt should transform into water-soluble sulphates according to thermodynamic stability diagrams. Analysis of the roasted battery scrap confirmed the presence of lithium in form of sulphates, whereas cobalt was in form of both sulphate and oxide. The roasted batteries were then used as feed in water leaching, where 95% of Li and 36% of Co were extracted. The low extraction yield of Co is in line with the XRD results, which showed that Co was only partially transformed to sulphate during the roasting step. The extraction yield of Mn reached 61%, which was contradictory to the initial predictions based on the thermodynamic stability of Mn-compounds in the roasting conditions.

The high recovery rate of Li and the relatively good recovery of Mn indicate that the removal of these metals from the battery scrap before further high-temperature treatment is possible, and with further optimisation of the roasting conditions, improved Mn recovery rates are expected. Apart from the roasting parameter optimisation, a second round of water leaching would most likely increase the recoveries of Li, Mn and possibly Co. The low recovery of cobalt in water leaching is actually not an issue, as it is further recovered in smelting process unlike Li and Mn. In our study, the water leaching residue was mixed with industrial Ni-slag and subjected to a laboratory-scale Ni-slag cleaning process conducted at 1350 °C, using biochar as a reductant. In the smelting process, the valuable metals Co, Ni and Cu heavily deported to the matte and metal alloy phases formed during reduction. The addition of Ni-concentrate to the smelting mixture had two clear benefits; it increased the deportment of valuables to matte and eliminated the formation of the iron-rich metal alloy on top of

the slag. The biochar used in this work, obtained by pyrolysing black pellets at 600 °C, was an effective reductant for metal oxides from both battery scrap and industrial Ni-slag.

During sulphation roasting at 850 °C in oxygen-containing gas atmosphere, graphite from the battery scrap reacted with oxygen, forming CO_2 emissions and resulting in the loss of graphite, which is also classified as a CRM. From the elemental recovery perspective, it could make sense to separate as much of the graphite as possible before the roasting process, using for example froth flotation. However, this would add another processing stage to the recycling process already containing several stages, leading to negative impacts on exergy efficiency for example. In the future, holistic studies should be conducted regarding the process investigated here as well as other possible processes in terms of economical viability, circularity, life-cycle assessment as well as exergy efficiency and exentropy analysis (Vierunketo *et al*, 2023).

ACKNOWLEDGEMENTS

This research work has been supported by the Business Finland BatCircle 2.0 project (Grant number 43830/31/2020), and the Academy of Finland's RawMatTERS Finland Infrastructure (RAMI) based at Aalto University, GTK and VTT.

REFERENCES

Attah-Kyei, D, Sukhomlinov, D, Tiljander, M, Klemettinen, L, Taskinen, P, Jokilaakso, A and Lindberg, D, 2023. A Crucial Step Towards Carbon Neutrality in Pyrometallurgical Reduction of Nickel Slag, *Journal of Sustainable Metallurgy,* 9:1759-1776.

Baum, Z J, Bird, R E, Yu, X, and Ma, J, 2022. Lithium-Ion Battery Recycling–Overview of Techniques and Trends, *ACS Energy Letters,* 7(2):712–719.

Biswas, J, Ulmala, S, Wan, X, Partinen, J, Lundström, M and Jokilaakso, A, 2023. Selective Sulfation Roasting for Cobalt and Lithium Extraction from Industrial LCO-Rich Spent Black Mass, *Metals* 13(2):358.

Brückner, L, Frank, J, and Elwert, T, 2020. Industrial Recycling of Lithium-Ion Batteries–A Critical Review of Metallurgical Process Routes, *Metals*, 10(8):1107.

Crundwell, F.K, Moats, M.S, Ramachandran, V, Robinson, T.G and Davenport, W.G, 2011. Chapter 18: Flash Smelting of nickel sulfide concentrates. In Extractive Metallurgy of Nickel, Cobalt, and Platinum-Group Metals; Elsevier: Kidlington, Oxford, UK, 2011; pp. 215–232.

Dańczak, A, Ruismäki, R, Rinne, T, Klemettinen, L, O'Brien, H, Taskinen, P, Jokilaakso, A and Serna-Guerrero, R, 2021. Worth from Waste: Utilizing a Graphite-Rich Fraction from Spent Lithium-Ion Batteries as Alternative Reductant in Nickel Slag Cleaning, *Minerals,* 11:784.

Grohol, M and Veeh, C, 2023. Study on the critical raw materials for the EU 2023: final report, European Commission, Directorate-General for Internal Market, Industry, Entrepreneurship and SMEs (Publications Office of the European Union) https://data.europa.eu/doi/10.2873/725585

Jochum, K P, Weiss, U, Stoll, B, Kuzmin, D, Yang, Q, Raczek, I, Jacob, D E, Stracke, A, Birbaum, K, Frick, D A, Günther, D and Enzweiler, J, 2011. Determination of Reference Values for NIST SRM 610–617 Glasses Following ISO Guidelines, *Geostandards and Geoanalytical Research,* 35:397–429.

Jochum, K P, Willbold, M, Raczek, I, Stoll, B and Herwig, K, 2005. Chemical Characterisation of the USGS Reference Glasses GSA-1G, GSC-1G, GSD-1G, GSE-1G, BCR-2G, BHVO-2G and BIR-1G Using EPMA, ID-TIMS, ID-ICP-MS and LA-ICP-MS, *Geostandards and Geoanalytical Research,* 29:285-302.

Li, M, Lu, J, Chen, Z and Amine, K, 2018. 30 Years of Lithium-Ion Batteries, *Advanced Materials,* 30(33):1800561.

Makuza, B, Tian, Q, Guo, X., Chattopadhyay, K and Yu, D, 2021. Pyrometallurgical options for recycling spent lithium-ion batteries: A comprehensive review, *Journal of Power Sources,* 491:229622.

Neumann, J, Petranikova, M, Meeus, M, Gamarra, J D, Younesi, R, Winter, M and Nowak, S, 2022. Recycling of Lithium-Ion Batteries—Current State of the Art, Circular Economy, and Next Generation Recycling, *Advanced Energy Materials*, 12:2102917

Pudas, J, Erkkilä, A and Viljamaa, J (AkkuSer Ltd), 2015. Battery Recycling Method, *US patent* US8979006B2.

Rinne, T, Klemettinen, A, Klemettinen, L, Ruismäki, R, O'Brien, H, Jokilaakso, A and Serna-Guerrero, R, 2022. Recovering Value from End-of-Life Batteries by Integrating Froth Flotation and Pyrometallurgical Copper-Slag Cleaning, *Metals*, 12:15.

Ruismäki, R, Rinne, T, Dańczak, A, Taskinen, P, Serna-Guerrero, R and Jokilaakso, A, 2020a. Integrating flotation and pyrometallurgy for recovering graphite and valuable metals from battery scrap, *Metals,* 10(5):680.

Ruismäki, R, Dańczak, A, Klemettinen, L. Taskinen, P, Lindberg, D and Jokilaakso, A, 2020b. Integrated battery scrap recycling and nickel slag cleaning with methane reduction, *Minerals,* 10:435.

Van Achterberg, E, Ryan, C G, Jackson, S E and Griffin, W L, 2001. Data reduction software for LA-ICP-MS: Appendix. In Laser ablation-ICP-Mass Spectrometry in the Earth Sciences: Principles and Applications; Short Course Series; Sylvester, P.J. Ed.; Mineralogical Association of Canada: Ottawa, ON, Canada. 239–243.

Vierunketo, M, Klemettinen, A, Reuter, M A, Santasalo-Aarnio, A, Serna-Guerrero, R, 2023. A multi-dimensional indicator for material and energy circularity: Proof-of-concept of exentropy in Li-ion battery recycling, *iScience*, 26(11):108237.